Single-domain shape anisotropy in near-macroscopic $Ni_{80}Fe_{20}$ thin-film rectangles

Yi Li,[a] Yiran Lu, and W. E. Bailey
Materials Science & Engineering, Department of Applied Physics & Applied Mathematics, Columbia University, New York, New York 10027, USA

(Presented 17 January 2013; received 22 October 2012; accepted 30 November 2012; published online 13 March 2013)

Shape anisotropy provides a simple mechanism to adjust the local bias field in patterned structures. It is well known that for ellipsoidal particles $<1\,\mu$m in size, a quasi-single domain state can be realized with uniform anisotropy field. For larger patterned ferromagnetic thin-film elements, domain formation is thought to limit the effectiveness of shape anisotropy. In our work, we show that very soft lithographically patterned $Ni_{80}Fe_{20}$ films with control of induced magnetic anisotropy can exhibit shape anisotropy fields in agreement with single-domain models, for both hysteresis loop measurements at low field and ferromagnetic resonance measurements at high field. We show the superiority of the fluxmetric form over the magnetometric form of anisotropy estimate for thin films with control dimensions from $10\,\mu$m to $150\,\mu$m and in-plane aspect ratios above 10. [http://dx.doi.org/10.1063/1.4794876]

Micron- and submicron-scale patterned ferromagnetic thin films are of interest for applications in magnetoelectronics.[1–3] Shape anisotropy, through finite aspect ratios of length to width, provides a convenient mechanism to adjust the internal field $H_D = -NM$ in these structures,[4] independent of induced anisotropy. In nanometer-dimension patterned structures, estimates of the demagnetizing factor from uniform (ellipsoidal) formulae[5] are considered to represent the anisotropic field well.[6]

In uniformly magnetized thin-film structures of $10\,\mu$m and greater lateral dimension, appropriate formulae to estimate demagnetizing fields are not as clear. Two forms for N have been proposed since the earliest treatments of the topic:[7–9] "magnetometric" and "fluxmetric (ballistic)," which are the volume average and area average over the midplane normal to $\vec{M}$, respectively. These two forms diverge for structures with very large aspect ratios of thickness b to in-plane dimensions a, c (thin-film limit).[10] Nevertheless, the magnetometric form is widely applied in the literature,[11,12] typically without recognition that alternate forms exist. We are not aware of prior attempts to validate either form through comparison with the other in fitting experimental data.

In this paper, we show that the fluxmetric form is in fact the superior form for the demagnetizing factor N in the thin-film limit. We have evaluated this formula both in the limit of saturated magnetization in high field, using variable frequency ferromagnetic resonance (FMR), and in low-field hysteresis, using magnetic optic Kerr effect (MOKE) measurement. We find agreement of H_D to 20% with a simple analytic limit of the formulae shown in Ref. 9. We find, on the other hand, that the magnetometric form is a very poor estimate for thin films, disagreeing with experimental data by a factor of four for the structures considered in this study.

Patterned Py films ($Ni_{80}Fe_{20}$) were deposited on Si substrates using magnetron sputtering with base pressure better than 3×10^{-9} Torr. The structure of the films was Si/SiO_2 substrate/Ta(5 nm)/$Ni_{80}Fe_{20}$(40 nm)/Ta(3 nm). Laser-direct-write photolithography at a resolution of $1\,\mu$m was used to fabricate rectangular stripe patterns (Figs. 1(a) and 1(b)), with short dimensions ranging from $10\,\mu$m to $150\,\mu$m. A $1500\,\mu\text{m} \times 1500\,\mu$m square was used as the unpatterned comparison. Induced magnetic anisotropy was introduced using an *in situ* quadrupole electromagnet setup[13] in UHV. A rotating field of $H_I = 150$ Oe was applied in phase to the rotating sample holder at 0.25 Hz during sputtering. The Py films were deposited together on two identically patterned substrates. The first substrate, denoted as "Py-parallel" (PP), was oriented such that H_I is parallel to the long axes of the elements. The second substrate, "Py-orthogonal" (PO), has the orthogonal orientation. The films were post-annealed at 250 °C in vacuum of 10^{-6} Torr for 1 h under a field of 4.0 kOe along the deposition field to strengthen the induced anisotropy.

The hysteresis loops of the stripe arrays on PP and PO were characterized via MOKE with the biasing field applied along the short axes. The size of the laser spot is close to the array dimension (1.5 mm). The two substrates were then cut into individual arrays using a dicing saw. The in-plane shape anisotropy of the arrays was then characterized by FMR. The samples were scanned along their long and short axes. The dispersion curves $\omega(H)$ of each array were acquired with rf frequency varying from 2 GHz to 26 GHz. The curves were fitted by the Kittel function:

$$f^2 = \mu_0^2\gamma^2/(2\pi)^2 \cdot (H_{ex} + H_A)(H_{ex} + H_A + M_s), \qquad (1)$$

where H_{ex} is the external biasing field, H_A is the anisotropy field, $\gamma/2\pi = 2.799\,\text{MHz/Oe} \cdot g_{eff}/2$, and $\mu_0 M_s$ is the saturation inductance. The differences of the anisotropic fields (ΔH_A) on the two axes are recorded in order to determine the shape anisotropy.

To estimate H_A and analyze the experimental data, consider a rectangular stripe with coordinate system defined in

[a]Author to whom correspondence should be addressed. Electronic mail:prc1988@gmail.com.

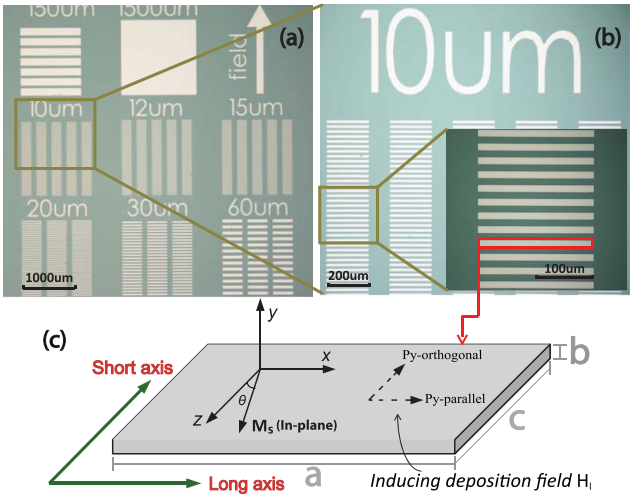

FIG. 1. (a,b) Patterned $Ni_{80}Fe_{20}$ stripe arrays with short dimensions ranging from 10 μm to 150 μm. The distances between adjacent stripes are the same as their widths. (c) Definition of Cartesian coordinates and the dimensions.

Fig. 1(c), with a, b, c as the long dimension, thickness, and short dimension along $\vec{x}, \vec{y}$ and $\vec{z}$ axes, respectively. We present a greatly simplified formula, N_{fs}, of the fluxmetric demagnetizing factor N_f from the full analytic form (Eq. (2) in Ref. 9), which could work as a substitute for N_f under thin film limit ($b \ll a, c$) and when the stripe is uniformly magnetized along $\vec{z}$

$$\pi N_{fs}^z = \frac{b}{ac}(\sqrt{4a^2 + c^2} - c) \approx \frac{b}{ac}(2a - c). \quad (2)$$

The second approximation is valid when the in-plane aspect ratio is large ($a \gg c$). When the magnetization is along $\vec{x}, N_{fs}^x$ is two orders of magnitude smaller than N_{fs}^z and does not contribute to the shape anisotropy. The full analytic formulae of N_f^z and N_m^z from Refs. 8 and 9 are compared in Fig. 2 along with N_{fs}^z for the thin film limit and a large in-plane aspect ratio (a/c = 20). We highlight the significant difference between calculated magnetometric and fluxmetric forms N_m and N_f, disagreeing with each other in the analytic calculation by a factor greater than three, as plotted in the inset of Fig. 2. We also highlight the accuracy of N_{fs} to the full fluxmetric form N_f: The filled circles are indistinguishable from the line in Fig. 2, disagreeing with each other by a maximum of 0.03% for the range considered in the calculation.

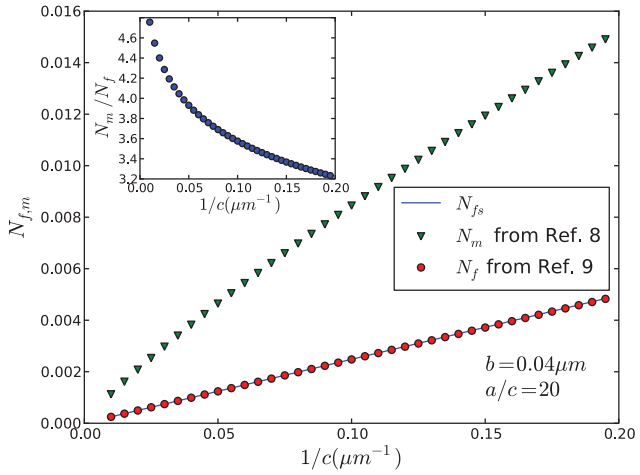

FIG. 2. Comparison of N_f, N_m, and N_{fs} in the thin-film limit and at large aspect ratio. Note the large divergence between N_f and N_m for wide samples (c > 5 μm). Inset: Ratio of N_m to N_f.

In an array of thin-film elements, additional dipolar fields arise from neighboring elements. The stray dipolar field H_s from the magnetostatic interaction can be calculated by summing up all the dipolar fields from the neighboring elements on each element and then taking an average of all the local fields. The stray field factor is defined as $H_s^{x,z} = -M_s N_s^{x,z}$, with the superscript denoting the magnetization direction. Parts of the calculated ΔN_f and ΔN_s are listed in Table I, with definition of $\Delta N_{f,s} = N_{f,s}^z - N_{f,s}^x$. In the structures ΔN_s is about a quarter of ΔN_f but with opposite sign, reducing the total demagnetizing field.

When the rectangular stripe defined in Fig. 1(c) is under an external field H_{ex} along $\vec{z}$, the total energy can be expressed as

$$E = -\mu_0 M_s H_{ex} \cos\theta + [\pm K + \frac{1}{2}\mu_0 {M_s}^2(\Delta N^* + \Delta N_s)]\cos^2\theta, \quad (3)$$

where K is the induced anisotropy energy, θ is the angle between $\vec{M}_s$ and $\vec{H}_{ex}$, and ΔN^* stands for either ΔN_m or ΔN_f. The sign of the induced anisotropy energy is positive for PP and negative for PO. In a classical model, $K = \mu_0 M_s H_{k0}/2$, where H_{k0} is the induced anisotropy field. The new saturation field with shape anisotropy becomes

$$H_k = \pm H_{k0} + M_s(\Delta N^* + \Delta N_s). \quad (4)$$

One should notice that when $H_k < 0$ the hysteresis loop will show easy-axis behavior.

In FMR, the effective anisotropy field can be calculated by $\vec{H}_A = -\partial E_A/\mu_0 \partial \vec{M}_s$ where E_A stands for the second term in Eq. (3). The magnetization of the elements in an array will precess about $\vec{H}_{ex}$ with small amplitudes. However because the movements of different elements are not in phase, the stray dipolar fields are decoupled from the resonance precession and we approximate them as a constant field. So in Eq. (3) the term $\frac{1}{2}\mu_0 {M_s}^2 \Delta N_s \cos\theta^2$ should be replaced by $\mu_0 {M_s}^2 N_s^i \cos\theta$, where N_s^i stands for the stray dipolar factor along the biasing field direction. The effective anisotropic fields along $\vec{x}$ and $\vec{z}$ are calculated to be

$$H_A^{x,[z]} = +, [-](\pm H_{k0} + M_s \Delta N^*) - M_s N_s^{x,[z]}. \quad (5)$$

At fixed frequency, the difference of the effective anisotropic field between $\vec{x}$ and $\vec{z}$ is

$$\Delta H_A = H_A^z - H_A^x = 2[\pm H_{k0} + M_s(\Delta N^* + \Delta N_s/2)]. \quad (6)$$

TABLE I. List of calculated ΔN_f and ΔN_s for dimensions. The equivalent anisotropic fields are calculated assuming $\mu_0 M_s = 0.95$ T.

Array (μm)	ΔN_f ($\times 10^{-4}$)	$M_s \Delta N_f$ (Oe)	ΔN_s ($\times 10^{-4}$)	$M_s \Delta N_s$ (Oe)
10	23.4	22.2	−5.8	−5.5
15	15.6	14.8	−4.0	−3.8
30	8.5	8.1	−2.0	−1.9
150	1.6	1.5	−0.7	−0.7

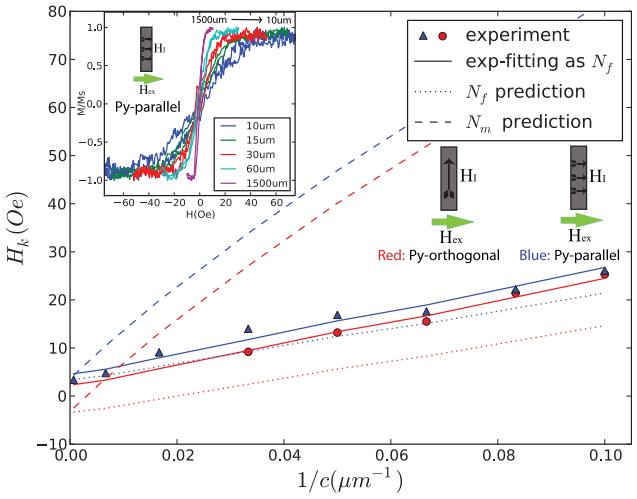

FIG. 3. Comparison of experimental H_k from MOKE with the prediction of N_f (dotted) and N_m (dashed) from Eq. (4) for PP and PO. Solid line: Data fitting into Eq. (4) by using N_f. Inset: Selected MOKE loops of PP arrays.

Figure 3 shows the experimental H_k from MOKE, in comparison with the analytic N_f (dotted) and N_m (dashed) from Eq. (4), as a function of 1/c. The experimental H_k of each array is obtained by extending the MOKE slopes at $H = 0$ to saturation. For PO arrays (not shown), when the stripe width is larger than 30 μm, H_k cannot be determined. The *inset* shows the hysteresis loops of PO arrays, all of which show linear H_A response with $H_c < 1$ Oe. The prediction curves are calculated taking the saturation inductance $\mu_0 M_s = 0.948$ T measured in FMR, and induced saturation field $H_{k0} = 3.4$ Oe measured from the 1500 μm $\times$ 1500 μm square.

The best fits to the MOKE-derived H_k are shown by the solid lines. Here, we treat $\mu_0 M_s$ and H_{k0} as free parameters but fit the two curves simultaneously. We find that the MOKE H_k values are close to the N_f prediction, and far from the N_m prediction. The data closely approximate the fitting lines to N_f, validating the simple approximate form in Eq. (4). The fitted $\mu_0 M_s$ is 1.17 T, 23% larger than 0.948 T. The fitted H_{k0} are 4.5 Oe (PP) and -2.3 Oe (PO). The former result is close to the 3.4 Oe but the latter is with an opposite sign. This is due to the domain wall movement rather than domain rotation and has also been discovered in patterned spin valves.[14]

Figure 4 shows the result of FMR measurement. In Fig. 4(a), the $f(H_{ex})$ relations with $\vec{H}_{ex}$ along $\vec{x}$ and $\vec{z}$ are fitted into Eq. (1) in order to extract g_{eff}, H_A, and $\mu_0 M_s$. All the arrays can be fitted well by the same $\mu_0 M_s$ of 0.948 T and g_{eff} of 2.115.

The differences in H_A are summarized in Fig. 4(b), in comparison with the analytic N_f (dotted) and N_m (dashed) from Eq. (6), as a function of $1/c$. The fitting into Eq. (6) is also completed with the same $\mu_0 M_s$ for the two series as the fitting parameters. Very close agreement between the experimental data and the fits is seen, with the fitting curves (solid lines) very close to the N_f prediction (dotted). The fitted H_{k0} are 4.7 Oe for PP and 3.1 Oe for PO, both close to the induced saturation field 3.4 Oe. The fitted $\mu_0 M_s$ is 1.08 T, 14% larger than 0.948 T from FMR.

We have shown that the fluxmetric demagnetizing factor N_f is superior to the magnetometric form N_m for large-area thin film rectangles (length/thickness > 200). Furthermore, we have shown a very simple analytical approximation, N_{fs}, to N_f in Eq. (2), which is excellent over the full range studied. These results will facilitate magnetostatic biasing of thin-film structures for applications in magnetoelectronics.

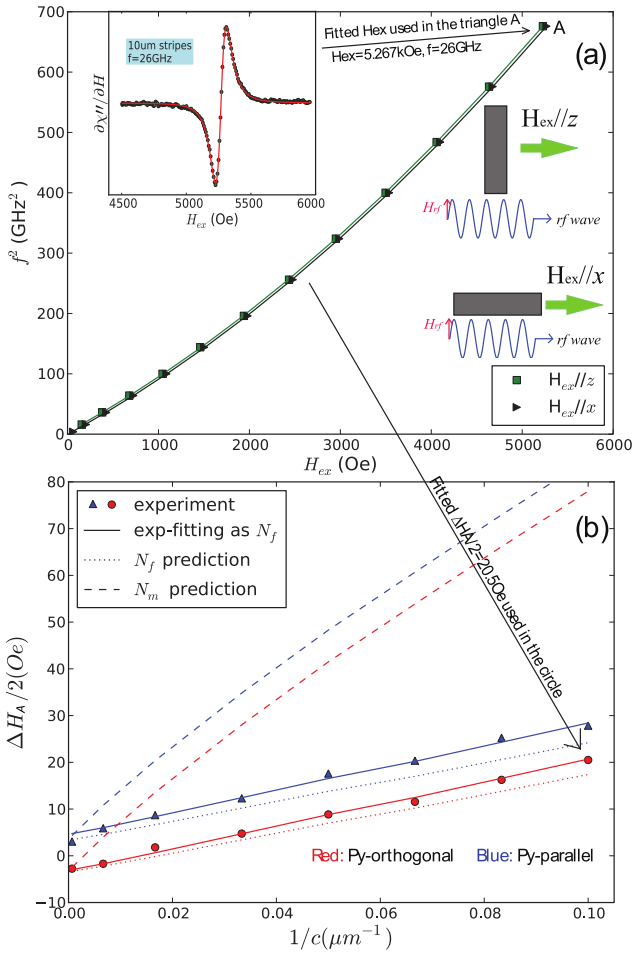

FIG. 4. (a) Fitting into Eq. (1) of the 10 μm PO array from in-plane FMR measurement with H_{ex} along $\vec{x}$ and $\vec{z}$ axis. Inset: Lineshape of the 10 μm PO array at 26 GHz. (b) Comparison of experimental ΔH_A from FMR with the prediction of N_f and N_m from Eq. (6) for PP and PO. Same notations as in Fig. 3.

We acknowledge support from the US Department of Energy Grant No. DE-EE0002892 and National Science Foundation No. ECCS-0925829.

[1]G. A. Prinz, Science **282**, 1660 (1998).
[2]S. A. Wolf, *et al.*, Science **294**, 1488 (2001).
[3]C. A. Ross, *et al.*, J. Appl. Phys. **91**, 6848 (2002).
[4]Y. Lu, *et al.*, Appl. Phys. Lett. **70**, 2610 (1997).
[5]J. A. Osborn, Phys. Rev. **67**, 351 (1945).
[6]M. Pardavi-Horvath, *et al.*, J. Appl. Phys. **110**, 053921 (2011).
[7]C. Riborg Mann, Phys. Rev. (Series I) **3**, 359 (1896).
[8]A. Aharoni, J. Appl. Phys. **83**, 3432 (1998).
[9]A. Aharoni, *et al.*, J. Appl. Phys. **87**, 6564 (2000).
[10]D. X. Chen, *et al.*, J. Appl. Phys. **91**, 5254 (2002).
[11]G. Shimon, *et al.*, Appl. Phys. Lett. **101**, 083112 (2012).
[12]Y. Zhuang, *et al.*, J. Appl. Phys. **99**, 08C705 (2006).
[13]C. Cheng, *et al.*, Rev. Sci. Instrum. **83**, 063903 (2012).
[14]Z. H. Qian, *et al.*, J. Appl. Phys. **109**, 103904 (2011).